Geochemistry Geophysics Geosystems G3

Technical Brief
Volume 13, Number 3
21 March 2012
Q03017, doi:10.1029/2011GC004027
ISSN: 1525-2027

Published by AGU and the Geochemical Society

A trio of laser ablation in concert with two ICP-MSs: Simultaneous, pulse-by-pulse determination of U-Pb discordant ages and a single spot Hf isotope ratio analysis in complex zircons from petrographic thin sections

Darren L. Tollstrup
Department of Geology, University of California, One Shields Avenue, Davis, California 95616, USA

Lie-Wen Xie
State Key Laboratory of Lithospheric Evolution, Institute of Geology and Geophysics, Chinese Academy of Sciences, PO Box 9825, Beijing 100029, China

Josh B. Wimpenny
Department of Geology, University of California, One Shields Avenue, Davis, California 95616, USA

Emily Chin and Cin-Ty Lee
Department of Earth Sciences, Rice University, Houston, Texas 77005, USA

Qing-Zhu Yin
Department of Geology, University of California, One Shields Avenue, Davis, California 95616, USA (qyin@ucdavis.edu)

[1] We have developed a technique for the simultaneous in situ determination of U-Pb ages and Hf isotope ratios from a single spot in complex, *discordant* zircons by combining both a single-collector and a multicollector sector field inductively coupled plasma–mass spectrometry (ICP-MS) with a 193 nm excimer laser ablation system. With a suite of zircon standards of various ages, we first show that U-Pb ages can be determined accurately to within 0.3–2.5% (2σ) compared to the nominal value, while the internal errors are better than 0.4–0.7%; hafnium isotope ratios are accurate, relative to solution analyses, within one epsilon unit, and internal errors are typically <0.008%. We then apply the technique to complex, discordant zircons with variable $^{206}Pb/^{238}U$ and $^{207}Pb/^{235}U$ ratios, commonly discarded previously as "un-reducible data," to construct a Discordia in U-Pb Concordia plot, using every scan, every laser pulse as individual data points from a single laser ablation spot (typically > 200–250 data points). We show that the upper and lower intercept ages from the Discordia, augmented by high precision Hf isotope data obtained on the same spot, reveal invaluable information that permit unique insight to geological processes not available by other means. We demonstrate that our technique is useful for provenance studies of small, complex detrital zircons in sedimentary and high-grade metamorphic rocks, in relation to crustal growth and evolution.

Components: 6700 words, 7 figures, 4 tables.

Keywords: geochronology; hafnium; isotopes; lead; uranium; zircon.

Index Terms: 1040 Geochemistry: Radiogenic isotope geochemistry; 1115 Geochronology: Radioisotope geochronology; 1194 Geochronology: Instruments and techniques.

Received 28 December 2011; **Revised** 6 February 2012; **Accepted** 6 February 2012; **Published** 21 March 2012.

Tollstrup, D. L., L.-W. Xie, J. B. Wimpenny, E. Chin, C.-T. Lee, and Q.-Z. Yin (2012), A trio of laser ablation in concert with two ICP-MSs: Simultaneous, pulse-by-pulse determination of U-Pb discordant ages and a single spot Hf isotope ratio analysis in complex zircons from petrographic thin sections, *Geochem. Geophys. Geosyst.*, *13*, Q03017, doi:10.1029/2011GC004027.

1. Introduction

[2] Zircon is the most widely used accessory mineral for determining the age, provenance, and thermal history of rocks. This is because zircons contain high concentrations of U, Th and Hf and are relatively resistant to later chemical alteration. Despite this, it has long been known that zircons are not immune to lead-loss, which results in discordant $^{206}Pb/^{238}U$ and $^{207}Pb/^{235}U$ ages [*Holmes*, 1954]. Various techniques and approaches have been developed in order to account for this lead loss in zircons and to achieve concordant U-Pb ages. These include the use of physical abrasion [*Krogh*, 1982a], magnetic separation [*Krogh*, 1982b], and chemical abrasion [*Mattinson*, 2005] techniques before zircon dissolution, U and Pb separation and isotopic analyses using a thermal ionization mass spectrometer (TIMS). These traditional approaches are sometimes capable of accounting for Pb-loss, but bulk dissolution is inappropriate and inapplicable to complexly zoned zircons. With the advent of in situ U-Pb dating techniques, such as secondary ion mass spectrometry [e.g., *Ireland and Williams*, 2003; *Li et al.*, 2009a], multiple concordant portions of zircons could be targeted for analysis while discordant zircons and metamict portions of zircons could be avoided through prior careful documentation of zircon domains with cathodoluminescence (CL) imaging.

[3] The use of laser ablation–inductively coupled plasma–mass spectrometry (LA-ICP-MS) has been demonstrated over the past decade as a rapid method with adequate precision for the U-Pb dating of U-rich minerals (e.g., zircon) and is becoming increasingly popular and widely applied [*Feng et al.*, 1993; *Fryer et al.*, 1993; *Hirata and Nesbitt*, 1995; *Horn et al.*, 2000; *Li et al.*, 2000, 2001; *Košler et al.*, 2002; *Jeffries et al.*, 2003; *Jackson et al.*, 2004; *Chang et al.*, 2006; *Gehrels et al.*, 2008; *Frei and Gerdes*, 2009]. Recently, the use of LA-multicollector-ICP-MS (LA-MC-ICP-MS) has gained increasing acceptance as a precise and accurate method for the in situ analysis of the Hf isotopic composition of zircons [*Thirlwall and Walder*, 1995; *Griffin et al.*, 2000, 2002; *Machado and Simonetti*, 2001; *Li et al.*, 2003; *Woodhead et al.*, 2004; *Iizuka and Hirata*, 2005; *Wu et al.*, 2006]. Recent studies by *Yuan et al.* [2008] and *Xie et al.* [2008] have even demonstrated a method for the simultaneous collection of data from a single laser system by splitting the ablated aerosol and measuring them simultaneously on two mass spectrometers. Using this method it is possible to collect U-Pb and/or trace element data together with Hf isotope data from the same laser ablation spot. However, all of these studies have focused on concordant zircons, or concordant domains within zoned zircons that are large enough to resolve spatially with laser ablation. *Gerdes and Zeh* [2009] presented a method for determining the upper and lower intercept ages for discordant and complexly zoned zircons, but this method requires multiple separate analyses of large (relative to the laser spot size) distinct growth and alteration zones within multiple zircon crystals extracted from a rock sample in order to construct lines of discordia. *Johnston et al.* [2009] present small volume (12–14 μm diameter, 4–5 μm depth) U-Pb zircon geochronology technique by LA-MC-ICP-MS. *Cottle et al.* [2009] showed a single shot laser ablation analysis could provide meaningful U-Pb ages on zircons with overgrowth rim, when a transient signal is fully integrated.

[4] The purpose of this study is to determine U-Pb ages and Hf isotope ratios from single spot analyses of complex, discordant zircons using laser ablation simultaneously coupled to a single-collector sector field HR-ICP-MS and a multiple-collector ICP-MS. We show that U-Pb datum could be obtained with ablation depth of ~60 nm in a single laser pulse and depth profiling of complex zircons are feasible. We monitored U/Pb elemental fractionation caused by differential volatility of U and Pb as laser ablation proceeds downhole. Using a suite of concordant zircon

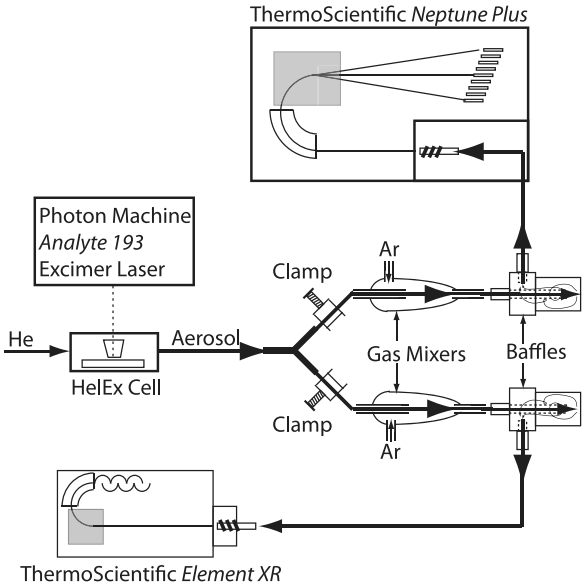

Figure 1. Schematic illustration of the trio: the experimental setup of a single spot laser ablation, and simultaneous determination of U-Pb ages (with the *Element XR* HR-ICP-MS) and high precision Hf isotope compositions on the *Neptune Plus* MC-ICP-MS.

standards, we show that the fractionation of U/Pb per unit time, dF/dt, can be taken as a constant for a given operational setting on the laser and ICP-MS. Correcting for U/Pb drift yielded U-Pb ages of zircon standards with accuracies to within 0.3–2.5% (2σ) that of nominal values and internal precisions of <0.4–0.7% (2σ). We used the same spot size and laser energy for all analyses within a single standard sample bracketed analytical session to ensure downhole fractionation of U/Pb observed for standards are applicable to unknown samples. In the case of discordant zircons, variations in time-resolved U/Pb during ablation are caused both by intrinsic heterogeneity during depth profiling and a baseline drift in the fractionation of U/Pb. The constant fractionation factor per unit time, dF/dt, as determined from external standards, was, therefore, used to subtract the baseline drift, leaving a residual signal that contains complex geochronologic information. We applied this approach to a suite of metamorphically overprinted detrital zircons from lower crustal meta-quartzite xenoliths sampled in late Miocene volcanics in the Sierra Nevada batholith, California. By treating each scan as an individual datum, we find that the time-resolved analyses systematically yield discordant arrays in a U-Pb Concordia plot. These zircons gave variable upper-intercept ages (1.7–2.8 Ga), typical of the cratonic basement ages of North American, but shared a common Cretaceous lower-intercept age (~100 Ma) to within error. The common lower-intercept age coincides with the peak of Cretaceous arc magmatism in the Sierra Nevada and, thus represent metamorphic overprinting of metasediments by magmatic heating. In contrast, Hf isotopes did not show resolvable zonation within uncertainty of measurements, allowing depleted mantle model ages to be determined in combination with U-Pb ages. In summary, this approach provides a means of extracting both juvenile crust formation ages and major crystallization and metamorphic events from a single zircon. In most laser ablation ICP-MS studies, where the entire signal is integrated, zircons found to be discordant are generally discarded because there is no means of extracting much age information, except for a minimum constraint on the upper-intercept age. The method presented here greatly expands the application of detrital zircon studies using U-Pb and Hf isotopes.

2. Experimental Setup and Data Acquisition

[5] Our setup for simultaneous U-Pb and Hf isotope analyses of zircons is similar to that described by *Yuan et al.* [2008] and *Xie et al.* [2008] but with the following important distinction. We use a different excimer laser ablation system (Photon Machines *Analyte 193H*) equipped with a dual volume sample cell (Photon Machines *HelEx Cell*), a single collector, magnetic sector field, high-resolution (HR)-ICP-MS (ThermoScientific *Element XR*) with high sensitivity compared to a conventional quadrupole ICP-MS, and a MC-ICP-MS (ThermoScientific *Neptune Plus*). This combination provides the most sensitive configuration for the purpose of this study. In brief, the sample aerosol created by the laser leaves the HelEx sample cell and is split into two paths using a y-connector, one destined for the *Element XR* and one for the *Neptune Plus* (see Figure 1). Gas mixers are used to introduce additional Ar make-up gas to the sample aerosol. The relative proportion of sample aerosol to each respective mass spectrometer has to be carefully controlled (between 1:9 to 3:7 proportion) to ensure both sufficient Hf signal for high precision isotopic analyses (>2.5 V on ^{180}Hf) on the *Neptune Plus*, as well as sufficiently high signal for U-Pb analyses on the *Element XR* in ion counting mode (^{238}U < 3 Mcps). Teflon baffles are used to increase signal

Table 1. Instrument Operating Parameters

	Description/Value for Laser Source	
Make	Photon Machines	
Model	*Analyte 193*	
Type	Excimer	
Wavelength	193 nm	
Repetition Rate	5–10 Hz	
Energy density	<5 J cm^{-2}	
Spot size	40–65 μm	
Pre-ablation	5 pulses	
	Description/Value	
	HR-SF-ICP-MS	MC-ICP-MS
Make	ThermoScientific	ThermoScientific
Model	*Element XR*	*Neptune Plus*
RF Power	1250 W	1250 W
Cooling Gas	15 L min^{-1}	15 L min^{-1}
Auxiliary Gas	0.8 L min^{-1}	0.8 L min^{-1}
Sample Gas (Ar)	1.4 L min^{-1}	1.3 L min^{-1}
Carrier Gas (He)	0.9 L min^{-1}	
Detector Mode	Counting	Faraday
Scan Mode	E-scan	Static

stability (while maintaining rapid washout times of < 2s) prior to introducing the aerosol into the plasma. A schematic representation of our experimental setup is provided in Figure 1, and all pertinent instrumental operating parameters are provided in Table 1.

[6] The Photon Machines *Analyte 193H* is a commercially available turn-key ArF excimer laser ablation system with a UV wavelength of 193 nm, maximum energy of 15 mJ at the sample surface, and a maximum pulse rate of 100 Hz. The high peak energy and short pulse duration of the *Analyte 193H* (4–5 ns compared to other excimer laser systems of 10–20 ns) minimizes the heat affected zone, providing cleaner ablations, improved ionization and reduced elemental fractionation. The laser ablation system includes a laser beam homogenizing system, a motor-controlled sampling stage with micrometer resolution, and coupled microscope and color CCD viewing system. The *Analyte 193H* produces homogeneous energy density at the site of ablation for a range of spot sizes up to 85 um in diameter that can be tuned by the user using an attenuator. Lower energies (4–5 mJ) and energy fluence (~1.2 Jcm^{-2}) resulted in increased signal stability and favorable downhole fractionation characteristics during this work. It has been well documented that 193 nm excimer laser ablation systems provide a more homogenous distribution of smaller particle sizes, which results in increased aerosol transmission and more efficient ionization within the ICP [*Eggins et al.*, 1998; *Gunther and Heinrich*, 1999]. A typical single pulse laser ablation crater achieved in our laboratory with *Analyte 193H* is shown in Figure 2a, with a crater depth of only ~60 nm/pulse (Figure 2b), and 350–400 nm for every 5 pulses (Figure 2c). This ensures our ability to perform chemical and isotopic analyses with depth profiling in oriented minerals with high spatial and depth resolution. Helium was used as a carrier gas to enhance aerosol transmission and to minimize deposition of ablated material [*Eggins et al.*, 1998; *Gunther and Heinrich*, 1999; *Jackson et al.*, 2004]. Our laser ablation system is equipped with a two-volume ANU-style *HelEx* sample cell. The small-volume inner cell of the *HelEx* cell results in the same rapid (<2 s) washout times of other small volume sample cells, while the large-volume primary sample cell allows for four standard thin sections, three 1 in. round mounts, and two 0.5 in. round mounts to be analyzed without opening the sample cell to atmosphere.

[7] The *Element XR* HR-ICP-MS was operated in low-resolution mode for U-Pb isotopes, which results in flat-top peaks and increased sensitivity (~2.5 Mcps for 1 ng/mL of ^{238}U in solution mode for an uptake rate of 50 μLmin^{-1} with an ESI PFA microflow nebulizer and cyclonic spray chamber), which is up to two orders of magnitude higher than what is obtainable with quadrupole mass spectrometers (cf. ~0.060 Mcps for 1 ng/mL of ^{238}U [*Yuan et al.*, 2008]). Average background intensities are negligible for high-mass isotopes (m/z > 85), and our gas backgrounds were lower relative to our increased sensitivity for all elements than those reported elsewhere [*Yuan et al.*, 2008]. The *Element XR* was tuned for maximum sensitivity and low-resolution mass calibrations were performed in solution mode daily. After connecting the laser, gas flows were adjusted for maximum sensitivity and signal stability. Depending on the size of the zircons being analyzed, U-Pb isotope data were acquired in time resolved mode using 30, 40, 50, or 65 μm spot sizes and parameters as shown in Table 2. Spot sizes and laser energy were also varied to limit the maximum signal of ^{238}U to < ~ 3 Mcps, as data were exclusively acquired in counting mode to avoid uncertainties associated with counting to analogue mode conversions. Total data acquisition times were 76 s, with 25–30 s of baseline acquisition before the laser was fired and

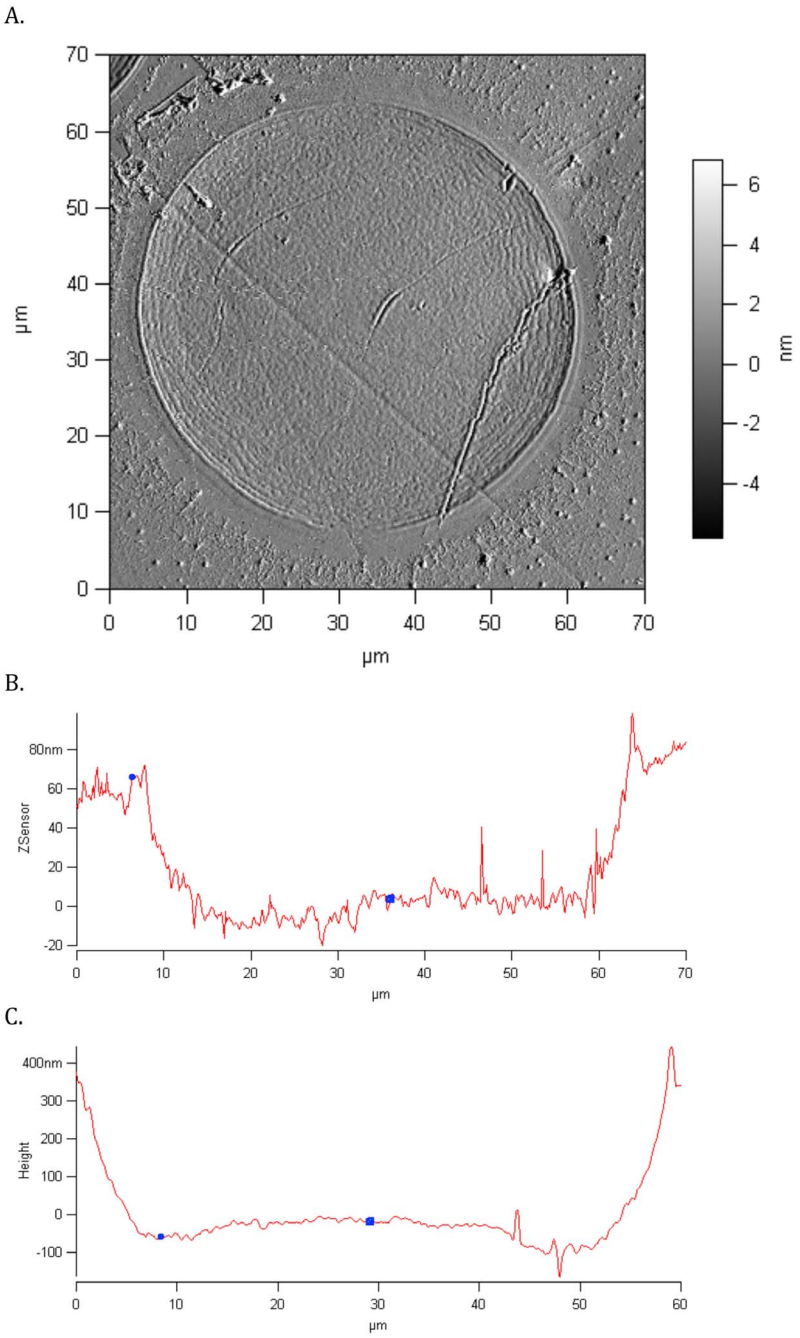

Figure 2. AFM (atomic force microscopy) image of (a) a single laser pulse on a zircon surface, and the depth profiles of laser craters, (b) ~60 nm/pulse and (c) ~350 nm/5 pulses.

~46–51 s of sample acquisition after the laser was fired (Figure 3). To improve sampling economy during the data acquisition, ^{202}Hg is not measured separately to correct ^{204}Hg on ^{204}Pb (Table 2). However, on peak baseline subtraction removes ^{204}Hg and any gas blank effectively. The resulting ^{204}Pb signal was found to be very low for all zircons in our study. A common lead correction scheme could be applied if necessary. Also ^{235}U is not measured separately (Table 2), instead ^{207}Pb/^{235}U ratio is calculated based on ^{207}Pb/^{206}Pb and ^{238}U/^{206}Pb measurements and assuming ^{238}U/^{235}U = 137.88. With such an optimized scheme, a total of 350 scans of data were acquired during the 76 s integration period (as shown in Figure 3), corresponding to ~0.21 s for each data point. For a

Table 2. Data Acquisition Parameters

	Description/Value
	HR-SF-ICP-MS
Isotopes measured	^{204}(Pb + Hg), ^{206}Pb, ^{207}Pb, ^{208}Pb, ^{232}Th, ^{238}U
Settling time	1 ms
Samples per peak	100
Mass window (%)	3
Sample Time	20 ms for ^{207}Pb, 10 ms for all other isotopes
Segment duration	60 ms for ^{207}Pb, 30 ms for all other isotopes
Cycles	350
Total time	76 s
	MC-ICP-MS
Isotopes measured	^{172}Yb, ^{173}Yb, ^{175}Lu, ^{176}Hf, ^{177}Hf, ^{178}Hf, ^{179}Hf, ^{180}Hf
Integration time	0.131 s
Settling time	3 s
Baseline type	On-Peak Zeros
Baseline duration	60 s

laser firing at a 5Hz repetition rate, each data point shown in Figures 3, 4 and 5 corresponds approximately to a single laser pulse. In the rare analysis where the laser was fired at 10Hz, each data point corresponds to signals integrated for every two pulses.

[8] The *Neptune Plus* MC-ICP-MS was operated in low resolution static multicollection mode using eight faraday collectors equipped with $10^{11}\Omega$ amplifier cards. The use of high-sensitivity sampler and skimmer cones (Jet-cone and X-cone, respectively) results in increased sensitivity ($\sim$1,400 Vppm^{-1} without the OnTool Booster Jet-Pump) relative to the earlier generation of *Neptune* (<400 Vppm^{-1}). The *Neptune Plus* was tuned for maximum sensitivity. Mass calibrations and detector gains were made in dry-plasma mode using an ESI *Apex IR* desolvating nebulizer prior to connecting to the laser. Once the laser was connected, gas flows were re-adjusted for maximum sensitivity and signal stability. Hafnium isotope data were acquired concurrent with the acquisition of U-Pb isotope data, using the

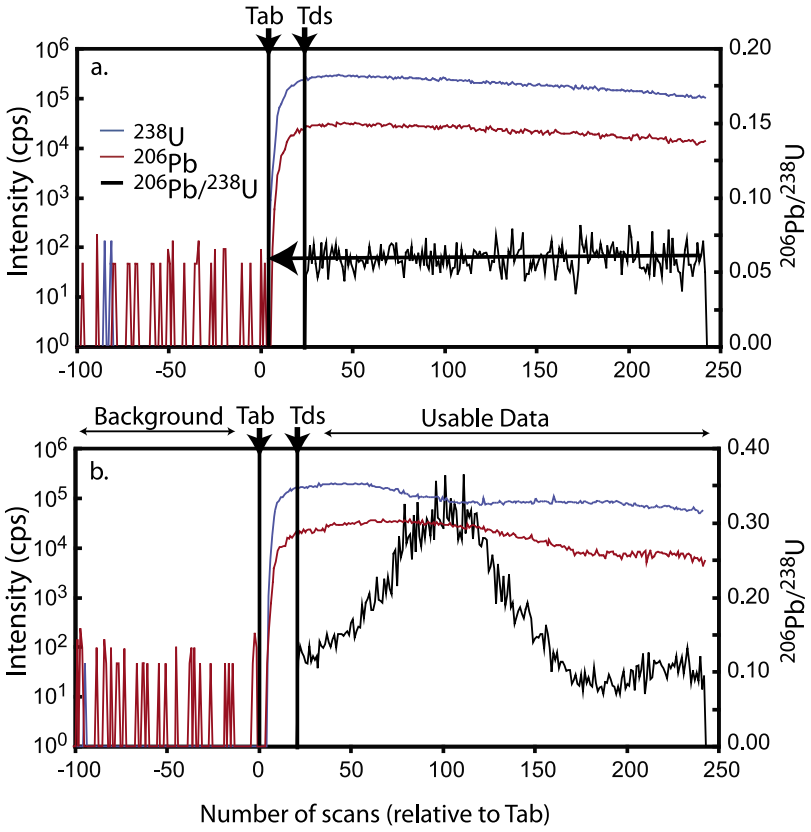

Figure 3. Representative time-resolved data acquired during laser ablation analysis of (a) a typical concordant zircon standard, and (b) small (40 μm) complexly zoned zircons showing variable Pb-loss, reflected in variable ^{206}Pb/^{238}U ratios. The total 350 scans acquired for each laser-ablated spot represent 76 s of total acquisition time. For a typical laser repetition rate 5 Hz, each scan shown in *x* axis corresponds roughly to signals generated for a single laser pulse.

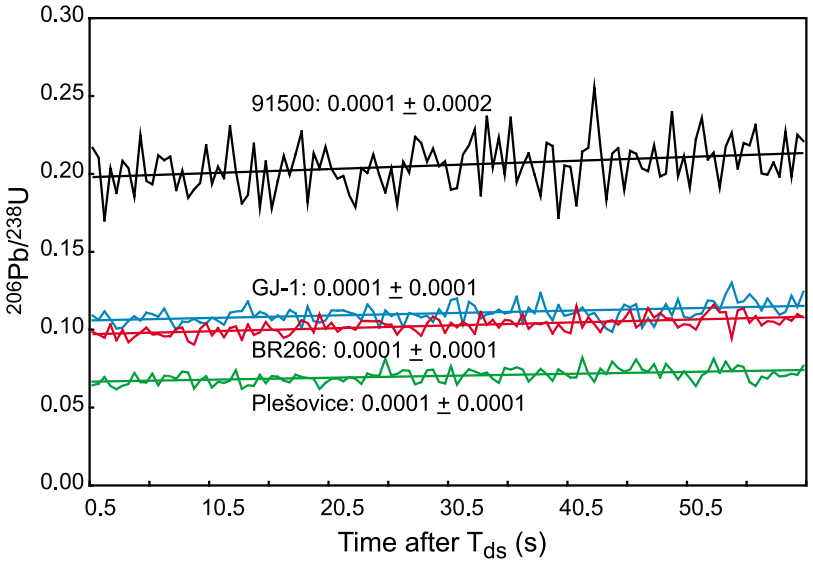

Figure 4. Time resolved $^{206}Pb/^{238}U$ ratios acquired during a single standard-sample bracketed analytical session. Each standard represents the average of 2 analyses, one at the beginning and one at the end of the session. Data for each standard are regressed and the resulting slopes are shown, with 2σ s.e. uncertainty.

parameters shown in Table 2. Typical ^{180}Hf signal intensities were >3–4 V for 91500.

[9] The following protocol is used for all zircon analyses. Individual standard sample bracketed sessions consist of 3 or more zircon standards with well-known U-Pb ages and Hf isotope compositions measured immediately before and after 5 unknown zircons. In this manner we can account for changes in elemental fractionation (U/Pb) and

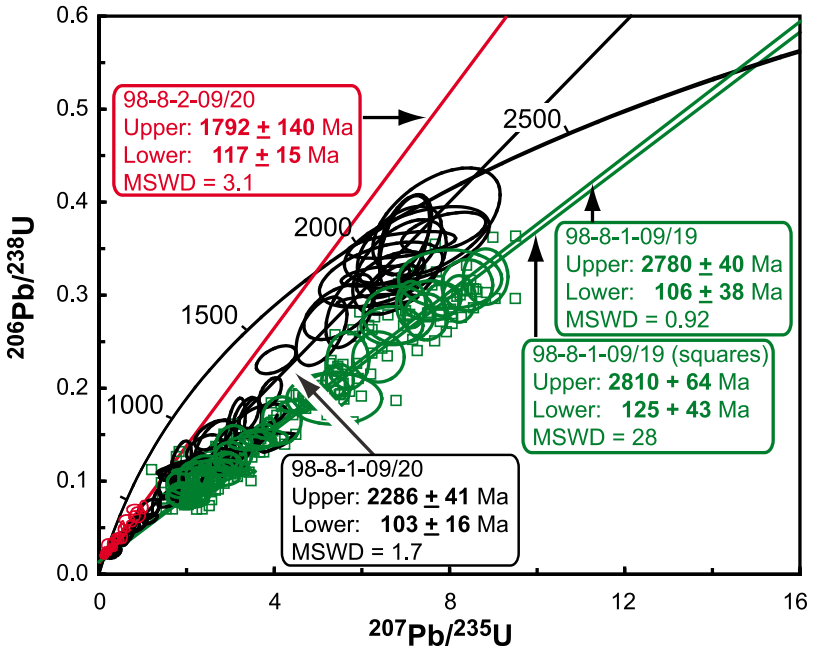

Figure 5. Concordia diagram showing the results of three representative complexly zoned and discordant zircons from a granulite-facies mid-crustal xenolith from the Sierra Nevada, CA. Results for all isotope data collected during a single laser ablation spot of sample 98-8-1-09/19 are shown green squares without errors, whereas results of integrated isotope data are shown as green error ellipses (2σ s.e.). Regressions of both sets of data performed using Isoplot yield identical upper and lower intercept ages, within quoted errors.

mass bias behavior that might occur over the duration of the session.

3. Data Reduction

[10] The typical time-resolved U-Pb isotope data acquisition procedures for zircons are shown in Figure 3. Baselines are acquired for ~25–30 s prior to firing the laser at time T_{ab}. Data collected during a 5s window between T_{ab} and T_{ds} are not used because the rapid increase in signal intensity and possible surface contamination result in widely variable isotope ratios. Only the data collected after the 5s window (starting at T_{ds}) are used in the data reduction and age calculations.

[11] For concordant zircons (which includes all of the standards), raw data are processed off-line using standard software packages of either *Iolite* or *Glitter*. For complexly zoned discordant zircons, an in-house Excel® spreadsheet program is used. Data reduction of all zircons begins with subtracting average baseline counts from the sample intensities measured during ablation. No common Pb correction has been applied to any of the data presented here as the background-corrected ^{204}Pb signals were below detection limit and $^{206}Pb/^{204}Pb$ ratios were greater than 1000. After baseline subtraction, elemental fractionation related to crater depth (referred to as downhole fractionation) is corrected by applying a least squares linear regression through all measured ratios of zircon standards back to T_{ab} (black line with arrow in Figure 3a).

[12] To illustrate our method for complex zircons, a time-resolved U-Pb isotope data acquisition from a small (~40 μm) anhedral and complexly zoned detrital zircon from a granulite facies lower crustal metasedimentary xenolith found in a Miocene diatreme in Sierra Nevada is shown in Figure 3b. The zircon is characterized by variable Pb loss. Whereas unzoned homogenous zircon standards are characterized by very stable $^{206}Pb/^{238}U$ ratios (Figures 3a and 4), zoned and variably discordant zircons contain significant isotopic variations (Figure 3b). Such isotopic heterogeneity is not amenable to traditional data reduction schemes such as Glitter and Iolite that are commonly used for concordant zircons. When faced with such a zircon with variable U/Pb ratio, the usual response is to either discard all of the data as "bad," or subjectively select portions of the data to regress and reduce using Glitter or Iolite. We have developed a different data reduction scheme for such cases (Figure 3b) that uses all of the available data from a single laser ablation spot to produce a line of discordia that results in meaningful upper and lower intercept ages.

[13] Our standard operating procedure ensures that the magnitude of change in downhole elemental fractionation (e.g., $^{206}Pb/^{238}U$) observed in each zircon is small (the slope of the regression shown in Figure 4 is within error of horizontal) and that different zircon reference materials all have the same magnitude of downhole fractionation, within error of the regression. Because we use the exact same spot size and laser energy for all analyses within a single standard sample bracketed analytical session, we can use the downhole fractionation determined for $^{206}Pb/^{238}U$ and $^{207}Pb/^{235}U$ from multiple zircon reference standards (Figure 4) to correct for the downhole fractionation of $^{206}Pb/^{238}U$ and $^{207}Pb/^{235}U$ induced by the laser on unknown zircons.

[14] Data reduction of complexly zoned zircons differs from that previously described for simple concordant zircons in the following manner. Multiple standards (typically 91500, Temora-1, BR-266, GJ-1, and M127a) are measured immediately before and after a set of 5 unknown zircons. After blank correction, downhole fractionation factors for $^{206}Pb/^{238}U$ and $^{207}Pb/^{235}U$ are calculated for each standard. These fractionation factors are evaluated on multiple zircon standards to ensure homogeneity (within the error of individual regressions) and the average of these downhole fractionation factors for $^{206}Pb/^{238}U$ and $^{207}Pb/^{235}U$ are calculated and then used to correct for the downhole fractionation of unknowns back to T_{ab} (e.g., Figure 3a). As shown in Figure 4, the downhole fractionation of U/Pb was linear with time, and identical within error for all zircon standards of homogeneous composition (changes in U/Pb ratio per unit time, dF/dt = constant). For unzoned zircons, this would result in a single $^{206}Pb/^{238}U$ and $^{207}Pb/^{235}U$ ratios, respectively. However, for complexly zoned zircons this approach preserves natural variability of a wide range of $^{206}Pb/^{238}U$ and $^{207}Pb/^{235}U$ ratios (Figure 3b). After this downhole fractionation correction in U/Pb, the intrinsic U/Pb variations of complex zircons (e.g., Figure 3b) during depth profiling could be uncovered.

[15] The average offset in the U/Pb ratio between the TIMS nominal value for zircon standard 91500 [*Wiedenbeck et al.*, 1995] and the measured value extrapolated to T_{ab} at the beginning and end of the analytical session is applied to correct further the

Table 3. In Situ U-Pb Ages Determined by LA-HR-ICP-MS Compared With Literature TIMS Data for Zircon Standards[a]

Standard Zircon	U-Pb Age (Ma) (This Study)	2σ (SE)	n	%	U-Pb Age (Ma) (TIMS)	2σ (SE)	References
GJ-1	598.2	2.2	41	−1.7	608.5	1.5	*Jackson et al.* [2004]
Plešovice	333.9	2.0	11	−0.9	337.1	0.4	*Sláma et al.* [2008]
Temora-1	416.7	2.6	19	0.0	416.8	1.1	*Black et al.* [2003]
B266 (z6266)	546.0	2.6	24	−2.3	559.0	0.2	*Stern and Amelin* [2003]
AS-3 (FC1)	1071.5	6.0	4	−2.5	1099.1	1.2	*Schmitz et al.* [2003]
M127	520.1	2.2	17	−0.8	524.3	0.5	*Mattinson* [2010]
Qinghu	160.0	2.0	2	0.3	159.5	0.2	*Li et al.* [2009a]
M257	568.3	3.8	5	1.2	561.4	0.5	*Nasdala et al.* [2008]

[a]2σ listed in the table represent 95% confidence level. Abbreviations: n, number of analyses obtained over the course of this study; %, percent deviation of the laser ablation data from the TIMS standard values.

instrumental mass bias to all other samples analyzed under the same operating parameters. Age determinations can then be made using all of the data points obtained from a single laser ablation spot (green squares in Figure 5; see auxiliary material for data and results presented in Figure 5) in Isoplot [*Lugwig*, 2003].[1] Although there are no errors associated with individual data points, it is possible to assign errors to individual data points based on counting statistics in order to use Isoplot and calculate mean square of weighted deviates (MSWD). Alternatively, each consecutive set of 5 measurements could be binned and averaged, allowing 2σ errors and estimates of error correlation (ρ) explicitly calculated and plotted using Isoplot to calculate discordant upper and lower intercept ages (error ellipses in green, black and red in Figure 5).

[16] Hafnium isotope data reduction follows that described by *Wu et al.* [2006]. Baselines are automatically subtracted from the sample data by the *Neptune* software. The baseline-corrected data is then further corrected for mass bias and isobaric interferences of ^{176}Yb and ^{176}Lu on ^{176}Hf offline in an Excel® spreadsheet, assuming exponential mass fractionation law of *Russell et al.* [1978] using ^{172}Yb/^{173}Yb = 1.35272, ^{176}Yb/^{172}Yb = 0.588673, and ^{176}Lu/^{175}Lu = 0.02655. Exponential mass bias correction of Hf isotopes assumes ^{179}Hf/^{177}Hf = 0.7325.

4. Results and Discussion

[17] Results of replicate analyses of zircon reference standards are provided in Table 3 and Figure 6. It shows that U-Pb ages obtained from homogenous zircons are accurate and reproducible to within 0.3–2.5% (2σ) compared to the TIMS value, while the internal errors are better than 0.4–0.7%. For the very young zircon (Qinghu), the internal error is 1.2%. Results of replicate analyses of ^{176}Hf/^{177}Hf ratios for the zircon standards are shown in Table 4 and Figure 6. Our laser ablation data reproduce the solution MC-ICP-MS values reported, all within one epsilon. Internal errors of individual laser ablation Hf isotope data are dependant upon factors such as signal intensity, laser spot size and energy, but typically are better than 0.000025 or (0.008%; 2σ s.e.) when ^{180}Hf intensities were greater than 2.5V.

[18] To test our method we present a combined U-Pb and Hf isotope data set for small (typically < 40 um) detrital zircons exposed in thick sections of mid- to lower-crustal metasedimentary xenoliths that occur in a Miocene diatreme erupted through the Sierra Nevada batholith. Results for three representative discordant zircons are presented in Figure 5. All three zircons are characterized by Cretaceous lower intercept ages that are within error of each other (103 Ma–125 Ma) suggesting the protolith materials were underthrusted to lower crustal depth at the peak of arc magmatism in the western USA. A range of upper intercept ages that vary from 1792 Ma to 2810 Ma are obtained, typical of North American cratonic basement. Ages calculated using all of the individual mass scan data (green squares) are identical within error to ages calculated using integrated data (the average of every 5 mass scans) (green ellipses). For example: upper and lower intercept ages calculated for zircon 98-8-1-09/19 (green data in Figure 5) are within error of each other. We should point out the laser ablation pit floor is rarely parallel to the true

[1]Auxiliary materials are available in the HTML. doi:10.1029/2011GC004027.

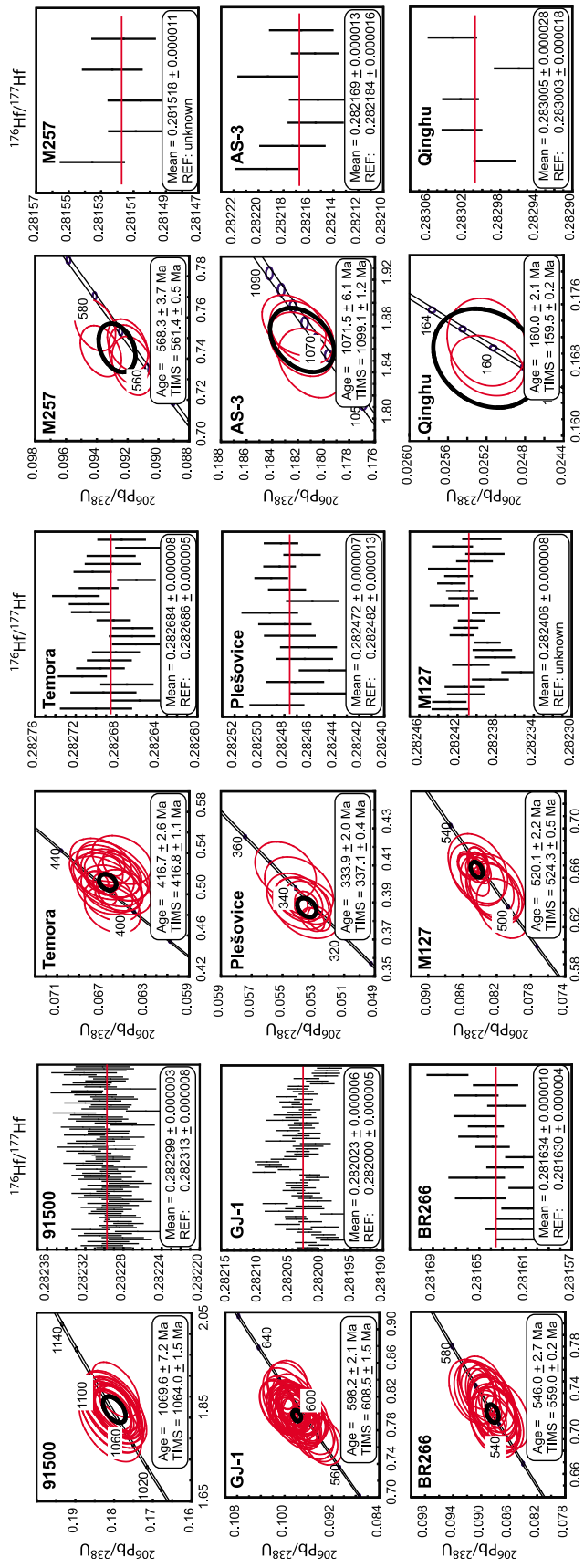

Figure 6. U-Pb and Hf isotope results of replicate analyses of zircon standards measured during this study. Large red error ellipses are 2σ (s.e.) for individual analyses, small blue error ellipse is 2σ s.e. for the mean Concordia ages calculated using Isoplot [*Ludwig*, 2003]. Data point error symbols for Hf isotope data are 2σ (s.e.). Interferences of ^{176}Yb and ^{176}Lu on ^{176}Hf are corrected assuming exponential mass bias using $^{172}Yb/^{173}Yb = 1.35272$, $^{176}Yb/^{172}Yb = 0.588673$, and $^{176}Lu/^{175}Lu = 0.02655$. Exponential mass bias correction of Hf isotopes assume $^{179}Hf/^{177}Hf = 0.7325$.

Table 4. Comparison of Hf Isotope Compositions of Zircon Standards Determined by Laser Ablation and Solution MC-ICP-MS[a]

Standard Zircon	$^{176}Hf/^{177}Hf$ (This Study)	2σ (SE)	n	$\varepsilon^{176}Hf$	2σ (SE)	$^{176}Hf/^{177}Hf$ Literature	2σ (SE)	Methods	References
Zircon 91500	0.282299	0.000003	83	−0.50	0.30	0.282313	0.000008	Solution	*Blichert-Toft* [2008]
GJ-1	0.282023	0.000006	53	0.82	0.28	0.282000	0.000005	Solution	*Morel et al.* [2008]
Plešovice	0.282472	0.000007	15	−0.35	0.53	0.282482	0.000013	Solution	*Sláma et al.* [2008]
Temora-1	0.282684	0.000008	22	−0.07	0.33	0.282686	0.000005	Solution	*Woodhead et al.* [2004]
B266 (z6266)	0.281634	0.000010	17	0.14	0.38	0.281630	0.000004	Solution	*Woodhead et al.* [2004]
AS-3 (FC1)	0.282169	0.000013	7	−0.53	0.73	0.282184	0.000016	Solution	*Woodhead and Hergt* [2005]
Qinghu	0.283005	0.000028	5	7.82	1.18	0.283003	0.000018	LA-ICPMS	*Li et al.* [2009b]
M127	0.282406	0.000008	19			not known			

[a]Abbreviations: n, number of repeat analyses obtained during the course of this study; $\varepsilon^{176}Hf$, parts per 10,000 deviation of the laser ablation data from the solution MC-ICP-MS values determined for the same standards.

age zonation of zircon of random orientation in a thin section. Results of our approach thus represent a variable degree of mixing of different age domains in a complex zircon. From the array of these discordant data points with variable degree of mixing, the age of initial zircon crystallization (the upper intercept) and the age of a younger zircon overgrowth or the age of a discrete open system event capable of partially resetting the U-Pb chronometer in zircon are uncovered. The common lower-intercept age in Figure 5 is significant and records the timing of a metamorphic event concomitant with peak arc magmatism in the Sierra Nevada (E. Chin et al., manuscript in preparation, 2012).

[19] The simultaneous collection of Hf isotope data coupled with U-Pb ages allows for further insights of crustal evolution history from the tiny zircon grains in the thin sections. Unlike the variable U/Pb ratio in the complex zircons, the Hf isotopic composition for the investigated zircons were uniform. This is consistent with previous work showing that the Hf isotope system is not modified by secondary processes that easily affect the U-Pb system [*Gerdes and Zeh*, 2009]. Figure 7a plots initial Hf isotopic compositions of zircons at the time of U-Pb lower and upper intercept ages in an Hf isotope evolution diagram, showing some zircons were crystallized from depleted upper mantle sources, while others were crystallized from enriched crustal sources. From merely 22 zircon grains examined in three petrographic thin sections, three episodes of juvenile crustal extraction at ∼3.2–2.3 Ga, ∼2.0–1.7 Ga, and 1.4 Ga from depleted upper mantle source are discernable. Using Hf isotope and Lu/Hf data, Hf model ages were calculated for each zircon, and plotted against U-Pb upper intercept ages (Figure 7b). Figure 7b highlights that crustal incubation time (or, crustal residence time, the dotted lines away from 1:1 correlation line) which suggest after juvenile crustal extraction from the depleted mantle sources, the chemical reservoirs evolve for another 300–1,500 Ma until zircons crystallize in the crustal settings (upper intercept ages). Figures 5 and 7 collectively highlight our method for analyzing complexly zoned and discordant zircons with single laser ablation spots for both U-Pb and Hf isotopes is robust and potentially widely applicable in zircon provenance and crustal growth and evolution studies.

5. Conclusions

[20] We present a variant for the simultaneous in situ determination of Hf and U-Pb isotope measurement applied to both concordant as well as complexly zoned zircons from a single laser spot during depth profiling. Results of U-Pb ages and Hf isotopes of large concordant zircon standards are both accurate and precise to within 1–2% and 0.008%, respectively. Additionally, we demonstrate the ability to measure the upper and lower intercept ages of small, complexly zoned, discordant zircons with similar levels of precision. These U-Pb ages augmented by the T_{DM} model ages determined from our simultaneous Hf isotope analyses, collectively provide a powerful means for the study of provenance, crustal growth and evolution.

Acknowledgments

[21] We thank the following individuals for providing various zircon standards used in this study: Lance Black, Bill Griffin, Carl Francis, Allen Kennedy, Xianhua Li, Dunyi Liu, Kevin McKeegan, Lutz Nasdala, and Jiří Sláma. We also thank Alan

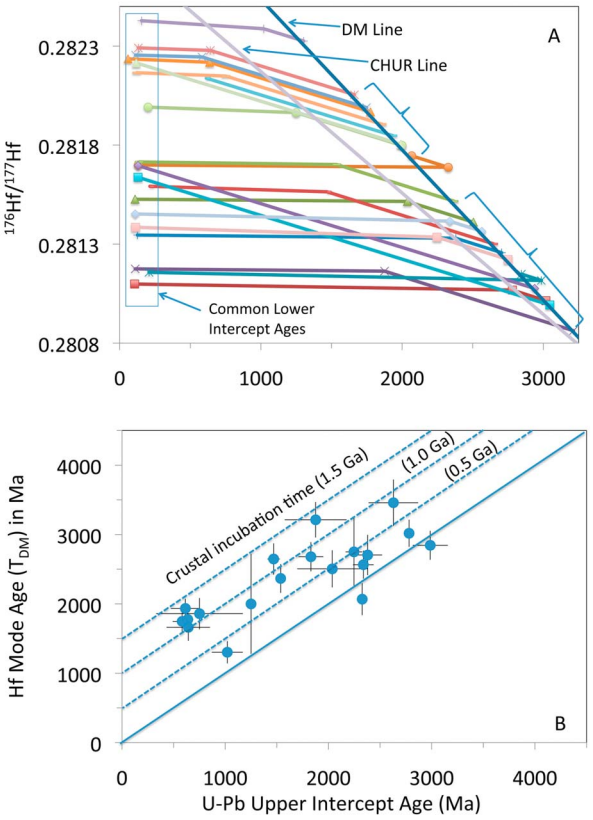

Figure 7. (a) Hf isotope evolution diagram for zircons measured in three different petrographic thin sections in metaquartzite xenoliths from Sierra Nevada batholith in California. Common lower intercept ages (L.I) at∼100 Ma for all zircons investigated are obvious. The kinks indicate the variable upper intercept ages (U.I.) of U-Pb concordia (Figure 5). The nearly horizontal lines connecting L.I. and U.I. indicate the generally low $^{176}Lu/^{177}Hf$ ratio of zircons. The common slope connecting the U.I. kink and the depleted mantle evolution (DM line) indicate the assumed average crustal $^{176}Lu/^{177}Hf$ ratio of 0.0115 [*Rudnick and Gao*, 2003]. The intercept with the DM line gives T_{DM} model age of crustal extraction. The DM line and chondritic uniform evolution line (CHUR line) are calculated assuming $(^{176}Hf/^{177}Hf)_{DM\ Today} = 0.283294$, $(^{176}Lu/^{177}Hf)_{DM} = 0.03933$ [*Vervoort and Blichert-Toft*, 1999], and $^{176}Hf/^{177}Hf_{CHUR\ today} = 0.282785$, and $^{176}Lu/^{177}Hf_{CHUR,today} = 0.0336$ [*Bouvier et al.*, 2008], respectively. T_{DM} are calculated using the terrestrial ^{176}Lu decay constant 1.867×10^{-11} [*Scherer et al.*, 2001]. (b) Hf model ages (T_{DM}) vs. U.I. ages of zircons. The offset from the 1:1 line in this diagram give a "crustal incubation" time (dotted lines) ranging from ∼300 Ma to 1,500 Ma from juvenile crustal extraction from the mantle (T_{DM}), until the crystallization of zircons in the crustal settings (U.I. ages).

Hicklin at the Spectral Imaging Facility of UC Davis for his help with the AFM image and depth profiling documentation of zircon after our laser ablation. Funding for the instruments used in this study are provided by NASA and the University of California Davis start-up funds to QZY. We sincerely acknowledge George Gehrels and another anonymous journal reviewer for their constructive comments and the editor Joel Baker for his efficient editorial handing of the manuscript.

References

Black, L. P., S. L. Kamo, C. M. Allen, J. N. Aleinikoff, D. W. Davis, R. J. Korsch, and C. Foudoulis (2003), TEMORA 1: A new zircon standard for Phanerozoic U–Pb geochronology, *Chem. Geol.*, *200*, 155–170, doi:10.1016/S0009-2541(03)00165-7.

Blichert-Toft, J. (2008), The Hf isotopic composition of zircon reference material 91500, *Chem. Geol.*, *253*, 252–257, doi:10.1016/j.chemgeo.2008.05.014.

Bouvier, A., J. D. Vervoort, and P. J. Patchett (2008), The Lu–Hf and Sm–Nd isotopic composition of CHUR: Constraints from unequilibrated chondrites and implications for the bulk composition of terrestrial planets, *Earth Planet. Sci. Lett.*, *273*, 48–57, doi:10.1016/j.epsl.2008.06.010.

Chang, Z., J. D. Vervoort, W. C. McClelland, and C. Knaack (2006), U-Pb dating of zircon by LA-ICP-MS, *Geochem. Geophys. Geosyst.*, *7*, Q05009, doi:10.1029/2005GC001100.

Cottle, J. M., M. S. A. Horstwood, and R. R. Parrish (2009), A new approach to single shot laser ablation analysis and its application to in situ Pb/U geochronology, *J. Anal. At. Spectrom.*, *24*, 1355–1364, doi:10.1039/b821899d.

Eggins, S. M., L. P. J. Kinsley, and J. M. G. Shelley (1998), Deposition and element fractionation processes during atmospheric pressure laser sampling for analysis by ICP-MS, *Appl. Surf. Sci.*, *127–129*, 278–286, doi:10.1016/S0169-4332(97)00643-0.

Feng, R., N. Machado, and J. Ludden (1993), Lead geochronology of zircon by laserprobe-inductively coupled plasma mass spectrometry (LP-ICPMS), *Geochim. Cosmochim. Acta*, *57*, 3479–3486, doi:10.1016/0016-7037(93)90553-9.

Frei, D., and A. Gerdes (2009), Precise and accurate *in situ* U-Pb dating of zircon with high sample throughput by automated LA-SF-ICP-MS, *Chem. Geol.*, *261*, 261–270, doi:10.1016/j.chemgeo.2008.07.025.

Fryer, B. J., S. E. Jackson, and H. P. Longerich (1993), The application of laser ablation microprobe-inductively coupled plasma-mass spectrometry (LAM-ICP-MS) to in situ (U)-Pb geochronology, *Chem. Geol.*, *109*, 1–8, doi:10.1016/0009-2541(93)90058-Q.

Gehrels, G. E., V. A. Valencia, and J. Ruiz (2008), Enhanced precision, accuracy, efficiency, and spatial resolution of U-Pb ages by laser ablation–multicollector–inductively coupled plasma-mass spectrometry, *Geochem. Geophys. Geosyst.*, *9*, Q03017, doi:10.1029/2007GC001805.

Gerdes, A., and A. Zeh (2009), Zircon formation versus zircon alteration—New insights from the combined U-Pb and Lu-Hf in-situ LA-ICP-MS analyses, and consequences for the interpretation of Archean zircon from the Central Zone of the Limpopo Belt, *Chem. Geol.*, *261*, 230–243, doi:10.1016/j.chemgeo.2008.03.005.

Griffin, W. L., N. J. Pearson, E. Belousova, S. E. Jackson, E. van Achterbergh, S. Y. O'Reilly, and S. R. Shee (2000),

The Hf isotope composition of cratonic mantle: LAM-MC-ICPMS analysis of zircon megacrysts in kimberlites, *Geochim. Cosmochim. Acta*, *64*, 133–147, doi:10.1016/S0016-7037(99)00343-9.

Griffin, W. L., X. Wang, S. E. Jackson, N. J. Pearson, S. Y. O'Reilly, X. S. Xu, and X. M. Zhou (2002), Zircon chemistry and magma genesis, SE China: In-situ analysis of Hf isotopes, Tonglu and Pingtan Igneous Complexes, *Lithos*, *61*, 237–269, doi:10.1016/S0024-4937(02)00082-8.

Gunther, D., and C. A. Heinrich (1999), Enhanced sensitivity in laser ablation-ICP mass spectrometry using helium-argon mixtures as aerosol carrier, *J. Anal. At. Spectrom.*, *14*, 1363–1368, doi:10.1039/a901648a.

Hirata, T., and R. Nesbitt (1995), U-Pb isotope geochronology of zircon: Evaluation of the laser probe-inductively coupled plasma mass spectrometry technique, *Geochim. Cosmochim. Acta*, *59*, 2491–2500, doi:10.1016/0016-7037(95)00144-1.

Holmes, A. (1954), The oldest dated minerals of the Rhodesian Shield, *Nature*, *173*, 612–614, doi:10.1038/173612a0.

Horn, I., R. L. Rudnick, and W. F. McDonough (2000), Precise elemental and isotope ratio determination by simultaneous solution nebulization and laser ablation-ICP-MS: Applications to U-Pb geochronology, *Chem. Geol.*, *167*, 405–425.

Iizuka, T., and T. Hirata (2005), Improvements of precision and accuracy in in-situ Hf isotope microanalysis of zircon using laser ablation-MC-ICPMS technique, *Chem. Geol.*, *220*, 121–137, doi:10.1016/j.chemgeo.2005.03.010.

Ireland, T. R., and I. S. Williams (2003), Considerations in zircon geochronology by SIMS, in *Zircon*, *Rev. Mineral. Geochem.*, vol. 53, edited by J. M. Hanchar, and P. W. O. Hoskin, pp. 215–241, Mineral. Soc. of Am., Washington, D. C.

Jackson, S. E., N. J. Pearson, W. L. Griffin, and E. A. Belousova (2004), The application of laser ablation-inductively coupled plasma-mass spectrometry (LA-ICP-MS) to in-situ U-Pb zircon geochronology, *Chem. Geol.*, *211*, 47–69.

Jeffries, T. E., J. Fernandez-Suarez, F. Corfu, and G. Gutierrez (2003), Advances in U-Pb geochronology using a frequency quintupled Nd:YAG based laser ablation system (λ = 213 nm) and quadrupole based ICP-MS, *J. Anal. At. Spectrom.*, *18*, 847–855, doi:10.1039/b300929g.

Johnston, S., G. Gehrels, V. Valencia, and J. Ruiz (2009), Small-volume U-Pb zircon geochronology by laser ablation-multicollector-ICP-MS, *Chem. Geol.*, *259*, 218–229, doi:10.1016/j.chemgeo.2008.11.004.

Košler, J., H. Fonneland, P. Sylvester, M. Tubrett, and R. B. Pedersen (2002), U-Pb dating of detrial zircons for sediment provenance studies—A comparison of laser ablation ICPMS and SIMS techniques, *Chem. Geol.*, *182*, 605–618, doi:10.1016/S0009-2541(01)00341-2.

Krogh, T. E. (1982a), Improved accuracy of U-Pb zircon ages by the creation of more concordant systems using the air abrasion technique, *Geochim. Cosmochim. Acta*, *46*, 637–649, doi:10.1016/0016-7037(82)90165-X.

Krogh, T. E. (1982b), Improved accuracy of U-Pb zircon ages by selection of more concordant fractions using a high gradient magnetic separation technique, *Geochim. Cosmochim. Acta*, *46*, 631–635, doi:10.1016/0016-7037(82)90164-8.

Li, X. H., X. Liang, M. Sun, Y. Liu, and X. Tu (2000), Geochronology and geochemistry of single-grain zircons: Simultaneous in situ analysis of U-Pb age and trace element by LAM-ICP-MS, *Eur. J. Mineral.*, *12*, 1015–1024.

Li, X. H., X. Liang, M. Sun, H. Guan, and J. G. Malpas (2001), Precise $^{206}Pb/^{238}U$ age determination on zircons by laser ablation microprobe-inductively coupled plasma-mass spectrometry using continuous linear ablation, *Chem. Geol.*, *175*, 209–219, doi:10.1016/S0009-2541(00)00394-6.

Li, X. H., X. R. Liang, G. J. Wei, and Y. Liu (2003), Precise analysis of zircon Hf isotopes by LAM-MC-ICPMS, *Geochim. Cosmochim. Acta*, *32*, 86–90.

Li, X. H., Y. Liu, Q. L. Li, C. H. Guo, and K. R. Chamberlain (2009a), Precise determination of Phanerozoic zircon Pb/Pb age by multicollector SIMS without external standardization, *Geochem. Geophys. Geosyst.*, *10*, Q04010, doi:10.1029/2009GC002400.

Li, X. H., W. X. Li, X. C. Wang, Q. L. Li, Y. Liu, and G. Q. Tang (2009b), Role of mantle-derived magma in genesis of early Yanshanian granites in the Nanling Range, South China: In situ zircon Hf-O isotopic constraints, *Sci. China, Ser. D*, *52*, 1262–1278, doi:10.1007/s11430-009-0117-9.

Ludwig, K. (2003), ISOPLOT: A geochronological toolkit for Microsoft Excel 3.00, *Spec. Publ. 4*, Berkeley Geochronology Cent., Berkeley, Calif.

Machado, N., and A. Simonetti (2001), U-Pb dating and Hf isotopic composition of zircon by laser ablation–MC-ICP-MS, in *Laser Ablation-ICPMS in the Earth sciences: Principles and Applications*, edited by P. Sylvester, pp. 121–146, Mineralogical Assoc. of Can., St. John's, Newfoundland.

Mattinson, J. M. (2005), Zircon U-Pb chemical abrasion ("CA-TIMS") method: Combined annealing and multi-step partial dissolution analysis for improved precision and accuracy of zircon ages, *Chem. Geol.*, *220*, 47–66.

Mattinson, J. M. (2010), Analysis of the relative decay constants of ^{235}U and ^{238}U by multi-step CA-TIMS measurements of closed-system natural zircon samples, *Chem. Geol.*, *275*, 186–198.

Morel, M. L. A., O. Nebel, Y. L. Nebe-Jacobsen, J. S. Miller, and P. Z. Vroon (2008), Hafnium isotope characterization of the GJ-1 zircon reference material by solution and laser-ablation MC-ICP-MS, *Chem. Geol.*, *255*, 231–235, doi:10.1016/j.chemgeo.2008.06.040.

Nasdala, L., et al. (2008), Zircon M257–A homogeneous natural reference material for the ion microprobe U-Pb analysis of zircon, *Geostand. Geoanal. Res.*, *32*, 247–265, doi:10.1111/j.1751-908X.2008.00914.x.

Rudnick, R. L., and S. Gao (2003), Composition of the Continental Crust, in *Treatise on Geochemistry*, vol. 3, *The Crust*, edited by R. L. Rudnick, pp. 1–64, Elsevier, Amsterdam.

Russell, W. A., D. A. Papanastassiou, and T. A. Tombrello (1978), Ca isotope fractionation on the Earth and other solar system materials, *Geochim. Cosmochim. Acta*, *42*, 1075–1090.

Scherer, E. E., C. Münker, and K. Mezger (2001), Calibration of the lutetium–hafnium clock, *Science*, *293*, 683–687, doi:10.1126/science.1061372.

Schmitz, M. D., S. A. Bowring, and T. R. Ireland (2003), Evaluation of Duluth Complex anorthositic series (AS3) zircon as a U-Pb geochronological standard: New high-precision isotope dilution thermal ionization mass spectrometry results, *Geochim. Cosmochim. Acta*, *67*, 3665–3672, doi:10.1016/S0016-7037(03)00200-X.

Sláma, J., et al. (2008), Plešovice zircon—A new natural reference material for U–Pb and Hf isotopic microanalysis, *Chem. Geol.*, *249*, 1–35, doi:10.1016/j.chemgeo.2007.11.005.

Stern, R. A., and Y. Amelin (2003), Assessment of errors in SIMS zircon U–Pb geochronology using a natural zircon standard and NIST SRM 610 glass, *Chem. Geol.*, *197*, 111–142, doi:10.1016/S0009-2541(02)00320-0.

Thirlwall, M. F., and A. J. Walder (1995), In-situ hafnium isotope ratio analysis of zircon by inductively coupled

plasma multiple collector mass spectrometry, *Chem. Geol.*, *122*, 241–247, doi:10.1016/0009-2541(95)00003-5.

Vervoort, J. D., and J. Blichert-Toft (1999), Evolution of the depleted mantle: Hf isotope evidence from juvenile rocks through time, *Geochim. Cosmochim. Acta*, *63*, 533–556, doi:10.1016/S0016-7037(98)00274-9.

Wiedenbeck, M., P. Allé, F. Corfu, W. L. Griffin, M. Meier, F. Oberli, A. von Quadt, J. C. Roddick, and W. Spiegel (1995), Three natural zircon standards for U-Th-Pb, Lu-Hf, and trace element and REE analyses, *Geostand. Newsl.*, *19*, 1–23, doi:10.1111/j.1751-908X.1995.tb00147.x.

Woodhead, J. D., and J. M. Hergt (2005), A preliminary appraisal of seven natural zircon reference materials for in situ Hf Isotope determination, *Geostand. Geoanal. Res.*, *29*, 183–195.

Woodhead, J., J. Hergt, M. Shelley, S. Eggins, and R. Kemp (2004), Zircon Hf-isotope analysis with an excimer laser, depth profiling, ablation of complex geometries, and concomitant age determination, *Chem. Geol.*, *209*, 121–135, doi:10.1016/j.chemgeo.2004.04.026.

Wu, F.-Y., Y.-H. Yang, L.-W. Xie, J.-H. Yang, and P. Xu (2006), Hf isotopic compositions of the standard zircons and baddeleyites used in U-Pb geochronology, *Chem. Geol.*, *234*, 105–126, doi:10.1016/j.chemgeo.2006.05.003.

Xie, L.-W., Y.-B. Zhang, H.-H. Zhang, J.-F. Sun, and F.-Y. Wu (2008), In situ simultaneous determination of trace elements, U-Pb and Lu-Hf isotopes in zircon and baddeleyite, *Chin. Sci. Bull.*, *53*, 1565–1573, doi:10.1007/s11434-008-0086-y.

Yuan, H.-L., S. Gao, M.-N. Dai, C.-L. Zong, D. Günther, G. H. Fontaine, X.-M. Liu, and C. R. Diwu (2008), Simultaneous determinations of U-Pb age, Hf isotopes and trace element compositions of zircon by excimer laser-ablation quadrupole and multiple-collector ICP-MS, *Chem. Geol.*, *247*, 100–118, doi:10.1016/j.chemgeo.2007.10.003.